Electronic Supplementary Material (ESI) for Chemical Communications.

Supporting Information

3D porous carbon networks with highly dispersed SiO_x by molecular-scale engineering toward stable lithium metal anodes

Zhitao Lu,‡ Shaohong Liu,‡ Chuanfa Li, Junlong Huang, Dingcai Wu, Ruowen Fu*

Materials Science Institute, PCFM Lab and GDHPPC Lab, School of Chemistry, Sun Yat-sen University, Guangzhou 510275, P. R. China.

‡These authors have contributed equally to this work.

Email: cesfrw@mail.sysu.edu.cn

Experimental section

1. Preparation of Br-modified CNT

In a typical synthesis, pristine CNT (5.7 g) was added to a mixture of 65% HNO_3 (174 ml) and H_2O (21 ml). The mixture was then reflux at 120 ºC for 28 h after dispersed by ultrasonication for 30 min, producing carboxyl groups functionalized CNT (CNT-COOH). Subsequently, the CNT-COOH was suspended in 60 ml of thionyl chloride and stirred at 70 ºC for 24 h to obtain carbonyl chloride group functionalized CNT (CNT-COCl). The CNT-COCl was then mixed with 120 mL of anhydrous glycol and stirred at 120 ºC for 48 h to obtain hydroxyl group functionalized CNT (CNT-OH). Afterwards, the CNT-OH (1.4 g) was dispersed in a mixture of anhydrous trichloromethane (35 mL), 4-dimethylaminopyridine (0.1 g) and triethylamine (1.5 mL). The dispersion was sealed in a flask in an ice/water bath and flushed with N_2 and then a solution of 2-bromo-2-methylpropionyl bromide (1.44 mL) dissolved in anhydrous trichloromethane (15 mL) was added dropwise in 30 min. The reaction was maintained at 0 ºC for 3 h and then at room temperature for 48 h to produce Br-modified CNT (CNT-Br).

2. Preparation of CNT-*g*-PTEPM

First, methacryloxypropyl triethoxysiliane (TEPM) was sealed in a bottle after flushing with N_2 for 15 min. Then, a Schlenk flask was charged with CNT-Br, CuBr, N,N,N',N'',N''-pentamethyldiethylenetriamine (PMDETA) and tetrahydrofuran (8 mL) and stirred for 0.5 h under gentle N_2 purge. TEPM was pulled out with a syringe and injected rapidly into the Schlenk flask. The solution was bubbled with N_2 for another 0.5 h, sealed and settled into a water bath of 50 °C. After 12 h, the reaction was stopped by opening the flask and exposing catalysts to air, giving rise to CNT-*g*-PTEPM. The molar ratio of TEPM/CNT-Br/CuBr/PMDETA was 100/1/5/5. The polymerization time could be increased to 24 h to achieve CNT@SiO_x-C with a higher content of SiO_x.

3. Preparation of CNT@SiO_x-C

Gelation of CNT-*g*-PTEPM was carried out by adding CNT-*g*-PTEPM into a mixed solution of ethanol (30 mL), distilled water (5 mL) and chlorhydric acid (37%, 5mL). CNT-*g*-*x*PTEPM was obtained after gelating for 1 day. Finally, the CNT-*g*-*x*PTEPM was annealed at 800ºC for 3h at a rate of 5ºC min^{-1} in flowing N_2, producing the target sample of CNT@SiO_x-C.

4. Structural characterizations

The nanostructures of the samples were observed by Hitachi S-4800 scanning electron microscope (SEM) and JEOL JEM-1400 Plus transmission electron microscope (TEM). Thermogravimetric analysis (TGA)

was performed by using PerkinElmer PE Pyris1 TGA thermogravimetric analyzer. Powder X-ray diffraction (XRD) patterns were recorded on a D-MAX 2200 VPC diffractometer using Cu K radiation. X-ray photoelectron spectroscopy (XPS) measurements were carried out with a Thermo SCIENTIFIC ESCALAB 250Xi instrument. Fourier-transform infrared (FTIR) measurements of the samples were performed with IR spectroscopy (Bruker TENSOR 27), using KBr disk method.

5. Electrochemical characterizations

The electrochemical performance of the samples was measured in 2032 coin cells. CNT@SiO_x/C and PVDF with a weight ratio of 9:1 were mixed in NMP and then casted onto Cu foil to prepare work electrodes. The mass loading of CNT@SiO_x/C in the typical electrode was around 0.5 mg cm^{-2}. Bare Cu foil and CNT electrode were used as the control working electrode for comparison. CR2032 coin cells were assembled with Celgard separators, Li foil (0.5 mm) counter electrodes and 40 μL electrolyte of 1.0 M LiTFSI in a mixture of DOL and DME (1:1 by volume) with 1 wt% $LiNO_3$ additive in an Ar-filled glove box. The cells aere first cycled from 0 to 1 V at 50 μA for 5 cycles to stabilize the SEI. After that, 1 mA h cm^{-2} of Li was deposited onto the working electrode at a current density of 1 mA cm^{-2}, followed by Li stripping away at the same current density with a cutoff voltage of 0.5 V. Typically, for the symmetrical cell test, 3 mA h cm^{-2} of Li was first plated onto the current collectors at 0.5 mA cm^{-2}, then the cells were cycled at the current density of 1 mA cm^{-2} for 1 h in each half cycle.

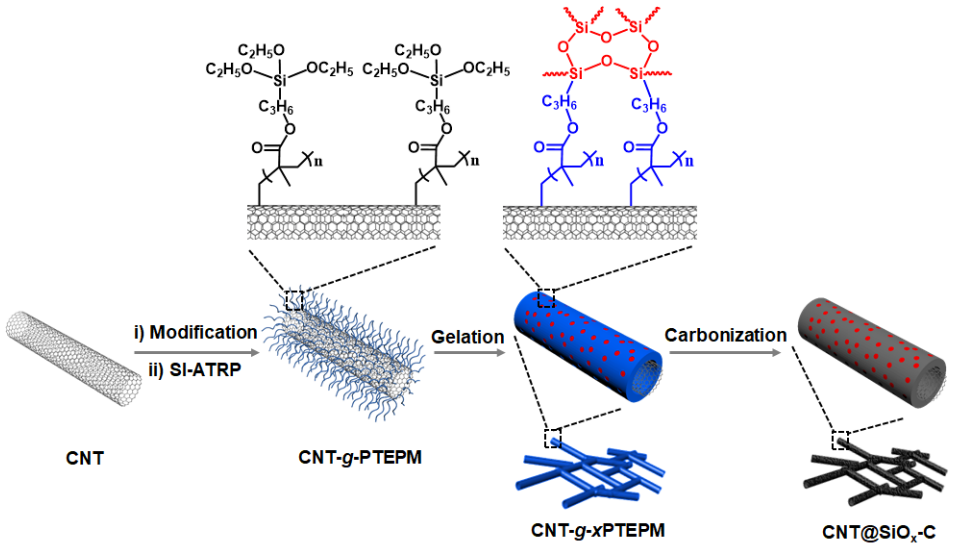

Fig. S1 Schematic representation of the procedure to prepare CNT@SiO_x-C.

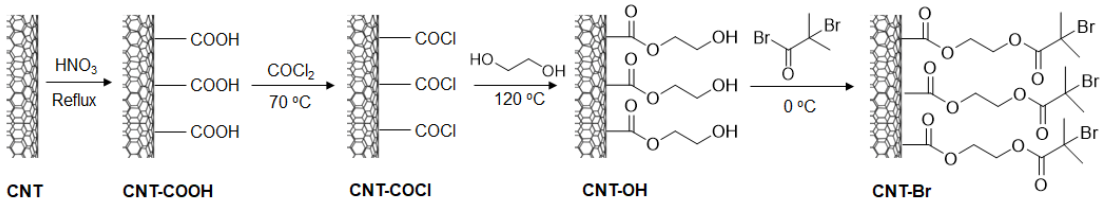

Fig. S2 Schematic representation of the procedure to prepare Br-modified CNT.

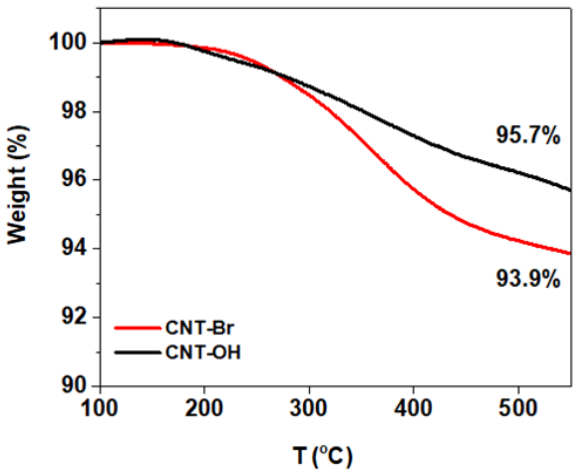

Fig. S3 TGA curves of CNT-OH and CNT-Br.

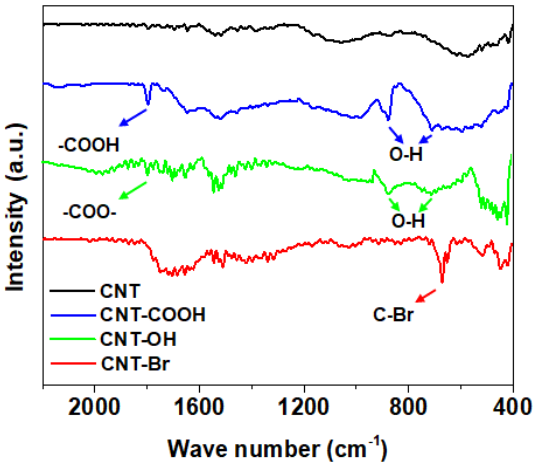

Fig. S4 FTIR spectra of CNT, CNT-COOH, CNT-OH and CNT-Br. The band at 1797 and board band at 1780-1625 cm^{-1} are assigned to the carbonyl stretch of the carboxylic acid group and ester bond[1]. The bands at 872 and 772 cm^{-1} are due to the O-H bending and out of phase O-H stretching[2]. The band observed at 670 cm^{-1} corresponds to C-Br stretching vibration in CNT-Br[3].

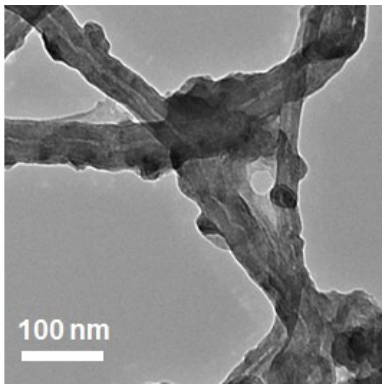

Fig. S5 TEM image of CNT-*g*-*x*PTEPM, revealing the nanonetworked structure.

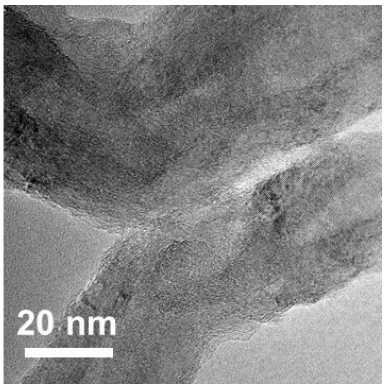

Fig. S6 TEM image of CNT@SiO_x-C.

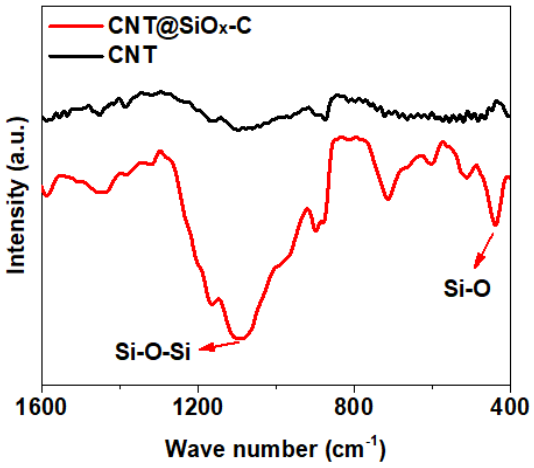

Fig. S7 FTIR spectra of the CNT@SiO_x-C and CNT.

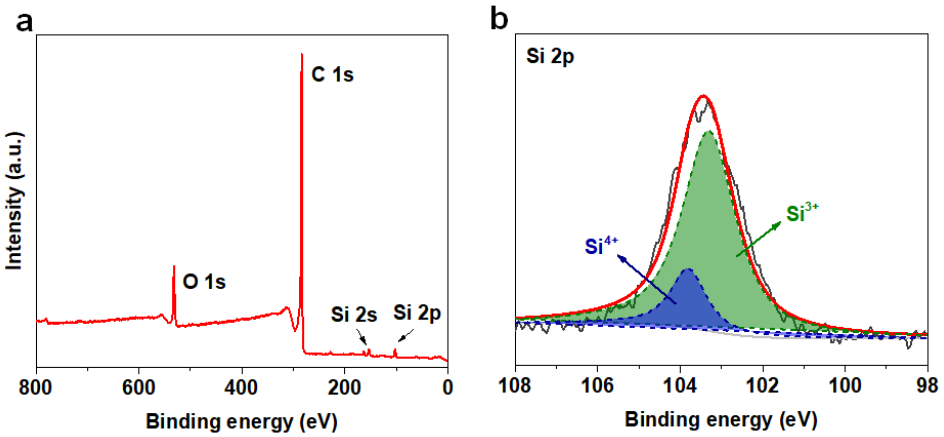

Fig. S8 (a) XPS full scan and (b) Si 2p high-resolution spectrum of CNT@SiO_x-C.

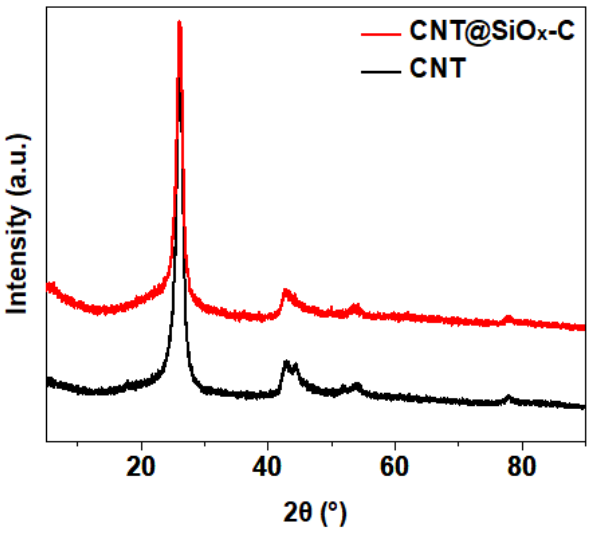

Fig. S9 XRD patterns of CNT@SiO_x-C and CNT.

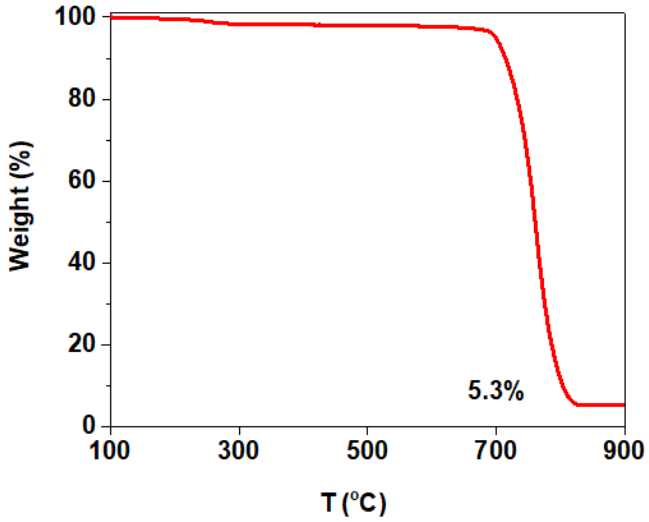

Fig. S10 TGA curve of synthesized CNT@SiO_x-C. According to the XPS result (Fig. S8), the average valence state of Si is estimated to be ~3.16 and the overall content of SiO_x in the CNT@SiO_x-C is calculated to be 4.7 wt%.

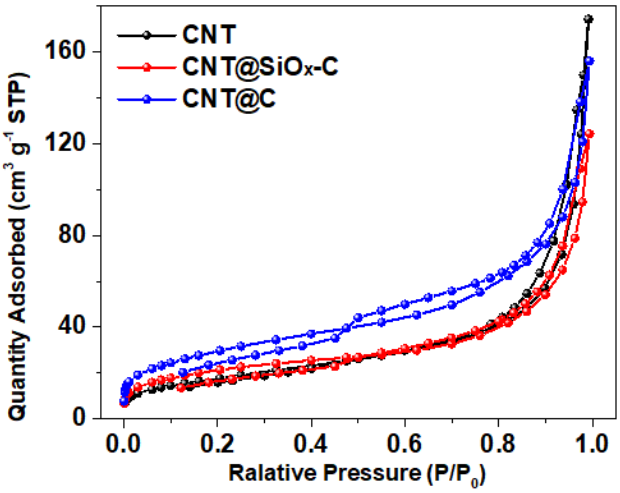

Fig. S11 (a) N_2 adsorption–desorption isotherms of CNT, CNT@SiO_x-C and CNT@C.

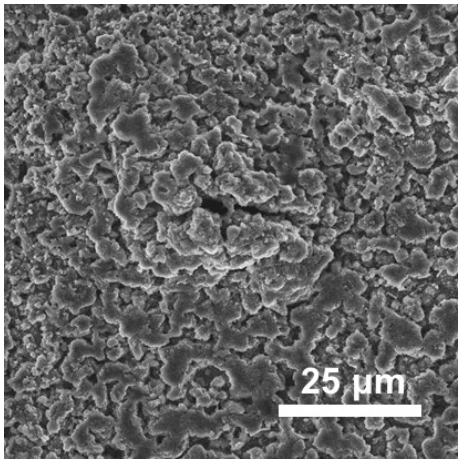

Fig. S12 Top-view SEM image of Cu electrode after plating 1 mA h cm^{-2} of Li.

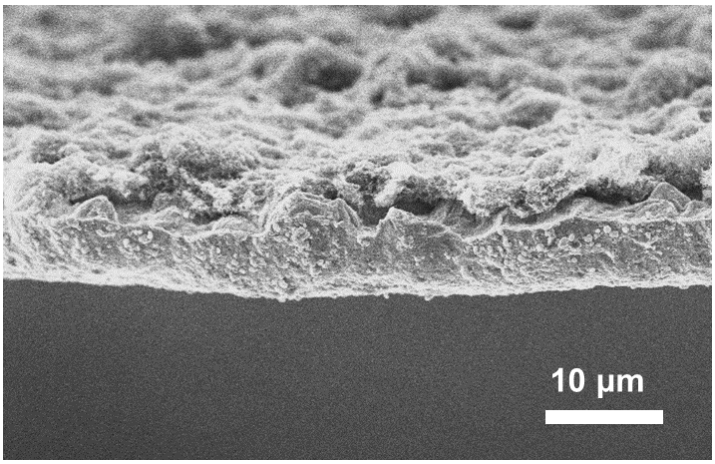

Fig. S13 Cross-section SEM image of CNT@SiO_x-C electrode.

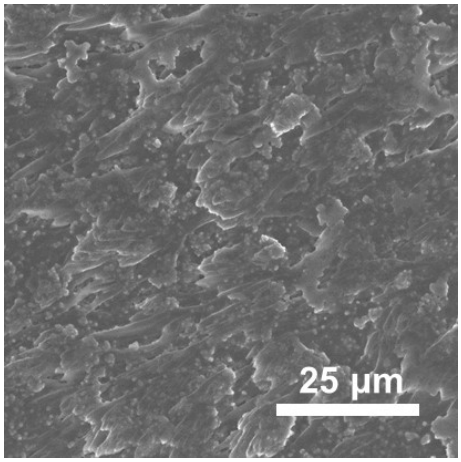

Fig. S14 Top-view SEM image of CNT@SiO_x-C electrode after plating 1 mA h cm^{-2} of Li.

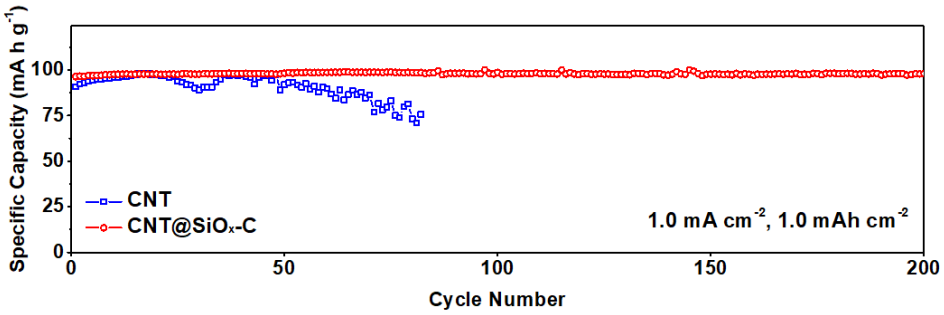

Fig. S15 Coulombic efficiencies of CNT and CNT@SiO_x-C electrodes with a capacity of 1 mA h cm^{-2} at 1 mA cm^{-2}.

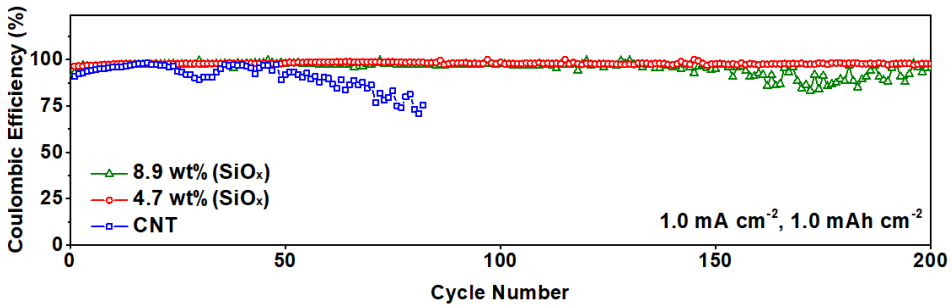

Fig. S16 Coulombic efficiencies of CNT and CNT@SiO_x-C electrodes with different contents of SiO_x with a capacity of 1 mA h cm^{-2} at 1 mA cm^{-2}. The CNT@SiO_x-C with 8.9 wt% of SiO_x is prepared by increasing the polymerization time of TEPM to 24 h.

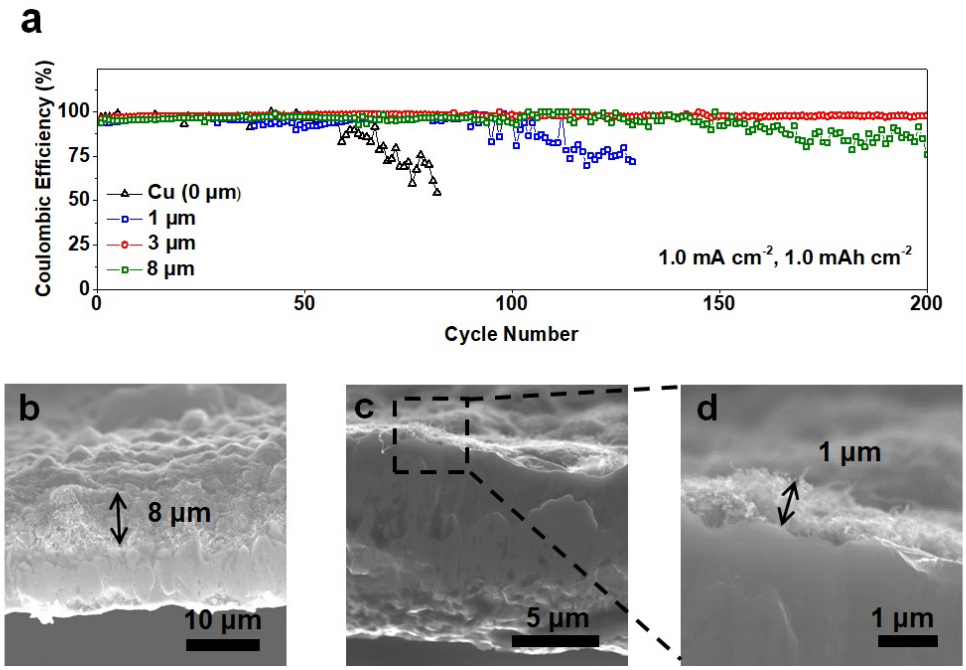

Fig. S17 (a) Coulombic efficiencies of CNT@SiO_x-C electrodes with different thicknesses of CNT@SiO_x-C layers on the Cu foil with a capacity of 1 mA h cm^{-2} at 1 mA cm^{-2}. Cross-section SEM images of CNT@SiO_x-C electrodes with different thicknesses of CNT@SiO_x-C layers: (b) 8 μm and (c, d) 1 μm. Coating an ultrathin layer of CNT@SiO_x-C (1 μm) can substantially increase the Li plating and stripping stability, indicating the great advantage of CNT@SiO_x-C as 3D host for dendrite-free Li deposition. Notably, further increasing the thickness of CNT@SiO_x-C from 3 to 8 μm can cause the deposition of Li on the surface of CNT@SiO_x-C and thus result in poor Li plating/stripping efficiencies[4].

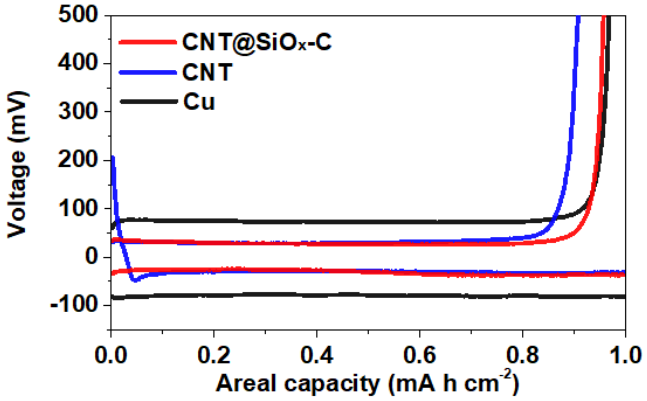

Fig. S18 The first galvanostatic cycling profiles of CNT@SiO_x-C, CNT and Cu electrodes at a current density of 1 mA cm^{-2}.

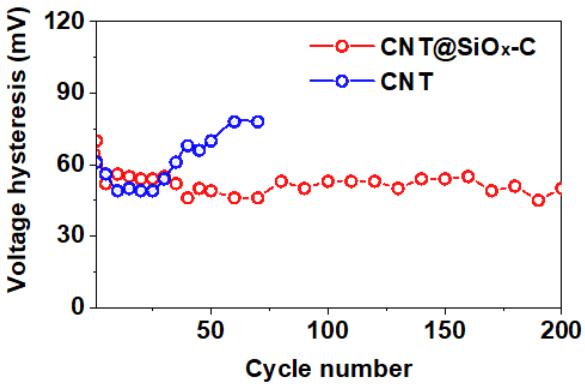

Fig. S19 Voltage hysteresis of Li plating/striping with CNT and CNT@SiO_x-C electrodes.

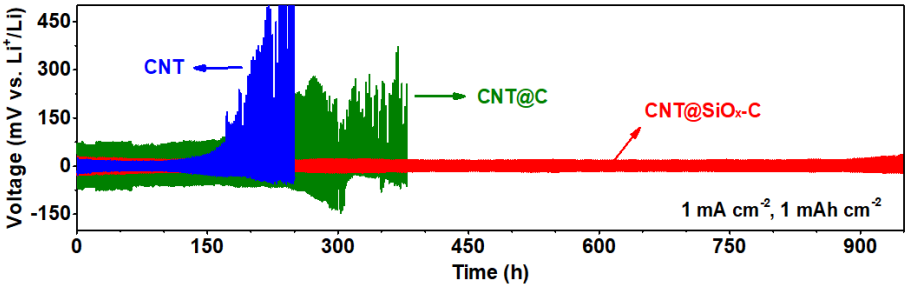

Fig. S20 Voltage–time profiles of the Li plating/stripping process with a cycling capacity of 1 mA h cm^{-2} at 1 mA cm^{-2} in symmetric Li|Li@CNT, Li|Li@CNT@C and Li|Li@CNT@SiO_x-C cells.

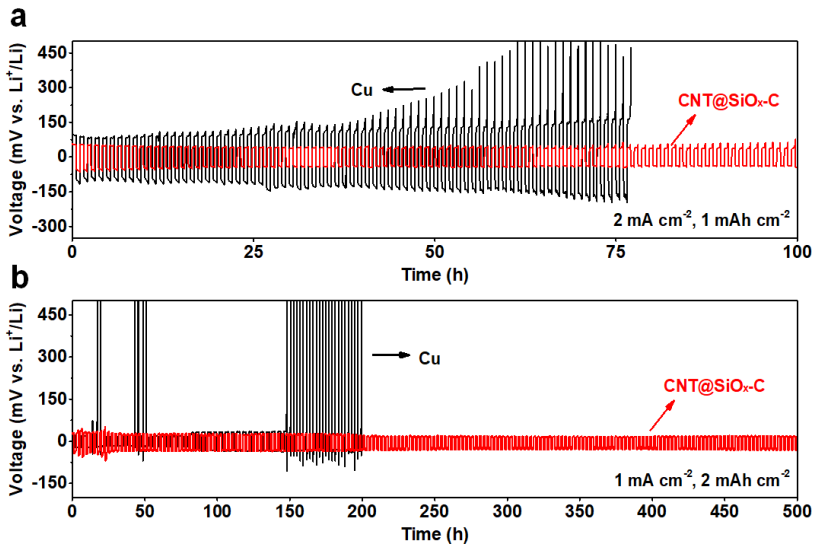

Fig. S21 Voltage–time profiles of the Li plating/stripping process with a cycling capacity of (a) 1 mA h cm^{-2} at 2 mA cm^{-2} and (b) 2 mA h cm^{-2} at 1 mA cm^{-2} in symmetric Li|Li@Cu and Li|Li@CNT@SiO_x-C cells.

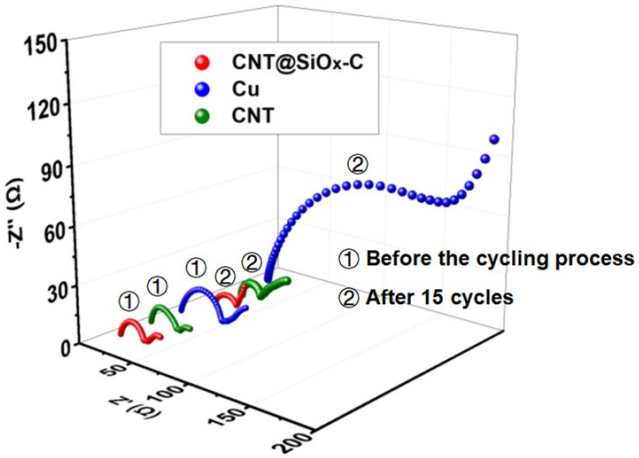

Fig. S22 Impedance spectra of the symmetric cells assembled with CNT@SiO_x-C, bare Cu and CNT electrodes before the cycling process and after 15 cycles.

Table S1. Electrochemical performance of the symmetric Li|Li@CNT@SiO_x-C cell in comparison with the previously reported Li hosts with large-sized lithiophilic species and other strategies for Li metal anodes

Strategies	Materials	Current density (mA cm^{-2})	Overpotential, (mV)	Time (h)	References
3D porous scaffolds	**CNT@SiO_x-C**	**1.0**	**40**	**950**	**This work**
	BNL (SiO_2)	1.0	86	700	5
	LCNE (SiO)	1.0	64	200	6
	PI-ZnO matrix (ZnO)	1.0	70	200	7
	Co–CS composite (Co_3O_4)	1.0	100	800	8
	cellular graphene scaffold	1.0	100	200	9
	Li/Al_4Li_9-LiF nanocomposite	1.0	90	50	10
Electrolyte additives	LiF	0.5	374	600	11
	$SiCl_4$	1.0	128	100	12
Separators	glass fiber cloths	1.0	78	160	13
	Al-coated garnet solid-state electrolyte separator	0.1	56	40	14
	PEO–LiTFSI-LLZO solid-state electrolyte separator	0.2	60	800	15
Artificial protective layers	polymeric grafted skin	0.5	60	300	16
	nanodiamonds	1.0	100	200	17
	organic-inorganic dual-layered interface	1.0	98	120	18
	LiF-coating layers	1.0	120	600	19

References

1. (a) I. V. Pavlidis, T. Tsoufis, A. Enotiadis, D. Gournis and H. Stamatis, *Adv. Eng. Mater.*, 2010, **12**, B179-B183; (b) L. Li, J. L. Davidson and C. M. Lukehart, *Carbon*, 2006, **44**, 2308-2315; (c) Z. Liu, S. Zhu, Y. Li, Y. Li, P. Shi, Z. Huang and X. Huang, *Polym. Chem-UK*, 2015, **6**, 311-321; (d) P. Kar and A. Choudhury, *Sensor Actuat. B-Chem.*, 2013, **183**, 25-33.
2. C. Y. Panicker, H. T. Varghese and D. Philip, *Spectrochim. Acta A*, 2006, **65**, 802-804.
3. (a) M. Karabacak, A. Çoruh and M. Kurt, *J. Mol. Struct.*, 2008, **892**, 125-131; (b) S. Ramalingam, P. Anbusrinivasan and S. Periandy, *Spectrochim. Acta A*, 2011, **78**, 826-834; (c) J. Swaminathan, M. Ramalingam, H. Saleem, V. Sethuraman and M. N. Ameen, *Spectrochim. Acta A*, 2009, **74**, 1247-1253.
4. H. Zhang, X. Liao, Y. Guan, Y. Xiang, M. Li, W. Zhang, X. Zhu, H. Ming, L. Lu and J. Qiu, *Nat. Commun.*, 2018, **9**, 3729.
5. S. Liu, L. Deng, W. Guo, C. Zhang, X. Liu and J. Luo, *Adv. Mater.*, 2019, **31**, e1807585.
6. D. C. Lin, J. Zhao, J. Sun, H. B. Yao, Y. Y. Liu, K. Yan and Y. Cui, *Proc. Natl. Acad. Sci. USA.*, 2017, **114**, 4613-4618.
7. Y. Y. Liu, D. C. Lin, Z. Liang, J. Zhao, K. Yan and Y. Cui, *Nat. Commun.*, 2016, **7**, 10992.
8. S. Li, Q. Liu, J. Zhou, T. Pan, L. Gao, W. Zhang, L. Fan and Y. Lu, *Adv. Funct. Mater.*, 2019, 1808847.
9. W. Deng, X. F. Zhou, Q. L. Fang and Z. P. Liu, *Adv. Energy Mater.*, 2018, **8**, 1703152.
10. H. S. Wang, D. C. Lin, Y. Y. Liu, Y. Z. Li and Y. Cui, *Sci. Adv.*, 2017, **3**, e1701301.
11. Y. Y. Lu, Z. Y. Tu and L. A. Archer, *Nat. Mater.*, 2014, **13**, 961-969.
12. L. Fan, H. L. Zhuang, W. D. Zhang, Y. Fu, Z. H. Liao and Y. Y. Lu, *Adv. Energy Mater.*, 2018, **8**, 1703360.
13. X. B. Cheng, T. Z. Hou, R. Zhang, H. J. Peng, C. Z. Zhao, J. Q. Huang and Q. Zhang, *Adv. Mater.*, 2016, **28**, 2888-2895.
14. K. K. Fu, Y. H. Gong, B. Y. Liu, Y. Z. Zhu, S. M. Xu, Y. G. Yao, W. Luo, C. W. Wang, S. D. Lacey, J. Q. Dai, Y. N. Chen, Y. F. Mo, E. Wachsman and L. B. Hu, *Sci. Adv.*, 2017, **3**, e1601659.

15. C. Z. Zhao, X. Q. Zhang, X. B. Cheng, R. Zhang, R. Xu, P. Y. Chen, H. J. Peng, J. Q. Huang and Q. Zhang, *Proc. Natl. Acad. Sci. USA.*, 2017, **114**, 11069-11074.

16. Y. Gao, Y. M. Zhao, Y. G. C. Li, Q. Q. Huang, T. E. Mallouk and D. H. Wang, *J. Am. Chem. Soc.*, 2017, **139**, 15288-15291.

17. X. B. Cheng, M. Q. Zhao, C. Chen, A. Pentecost, K. Maleski, T. Mathis, X. Q. Zhang, Q. Zhang, J. J. Jiang and Y. Gogotsi, *Nat. Commun.*, 2017, **8**, 336.

18. C. Yan, X. B. Cheng, Y. Tian, X. Chen, X. Q. Zhang, W. J. Li, J. Q. Huang and Q. Zhang, *Adv. Mater.*, 2018, **30**, 1707629.

19. J. Zhao, L. Liao, F. F. Shi, T. Lei, G. X. Chen, A. Pei, J. Sun, K. Yan, G. M. Zhou, J. Xie, C. Liu, Y. Z. Li, Z. Liang, Z. N. Bao and Y. Cui, *J. Am. Chem. Soc.,* 2017, **139**, 11550-11558.